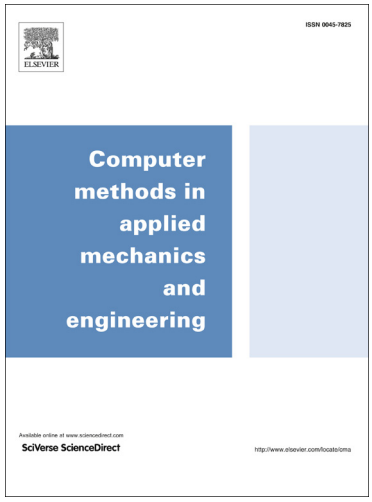

A multiscale quasicontinuum method for lattice models with bond failure and fiber sliding

L.A.A. Beex, R.H.J. Peerlings, M.G.D. Geers

PII: S0045-7825(13)00279-X
DOI: http://dx.doi.org/10.1016/j.cma.2013.10.027
Reference: CMA 10092

To appear in: *Comput. Methods Appl. Mech. Engrg.*

Received Date: 23 January 2013
Revised Date: 29 September 2013
Accepted Date: 21 October 2013

Please cite this article as: L.A.A. Beex, R.H.J. Peerlings, M.G.D. Geers, A multiscale quasicontinuum method for lattice models with bond failure and fiber sliding, *Comput. Methods Appl. Mech. Engrg.* (2013), doi: http://dx.doi.org/10.1016/j.cma.2013.10.027

A multiscale quasicontinuum method for lattice models with bond failure and fiber sliding

L.A.A. Beex*, R.H.J. Peerlings, M.G.D. Geers

Department of Mechanical Engineering, Eindhoven University of Technology, P.O. Box 513, 5600 MB Eindhoven, The Netherlands

Abstract

Structural lattice models incorporating trusses and beams are frequently used to mechanically model fibrous materials, because they can capture (local) mesoscale phenomena. Physically relevant lattice computations are however computationally expensive. A suitable multiscale approach to reduce the computational cost of large-scale lattice computations is the quasicontinuum (QC) method. This method resolves local mesoscale phenomena in regions of interest and coarse grains elsewhere, using only the lattice model. In previous work, a virtual-power-based QC framework is proposed for lattice models that include local dissipative mechanisms. In this paper, the virtual-power-based QC method is adopted for lattice models in which bond failure and subsequent frictional fiber sliding are incorporated - which are of significant importance for fibrous materials such as paper, cardboard, textile and electronic textile. Bond failure and fiber sliding are nonlocal dissipative mechanisms and to deal with this nonlocality, the virtual-power-based QC method is equipped with a mixed formulation in which the kinematic variables as well as the internal history variables are interpolated. Previously defined summation rules can still be used to sample the governing equations in this QC framework. Illustrative examples are presented.

Key words: lattice model, bond failure, quasicontinuum method, multiscale, fiber, friction, paper, cardboard, textile, electronic textile

*Corresponding author
Email: L.A.A.Beex@gmail.com

1. Introduction

Structural lattice models and discrete networks using trusses and beams are often used for the mechanical modeling of fibrous materials with discrete fibers and yarns at the mesoscale and microscale (Hou et al., 2009; Ngan, 2009; Hatami-Marbini and Picu, 2009; Ryvkin and Slepyan, 2010; Cui et al., 2011; Ridruejo et al., 2010; Zeman et al., 2011; Silberstein et al., 2012). They are typically used to model biological materials (Arnoux et al., 2002; Chandran and Barocas, 2006; Stylianopoulos and Barocas, 2007; Intrigila et al., 2007; Argento et al., 2012), paper networks (Bronkhorst, 2003; Batchelor, 2008; Liu et al., 2010; Strömbro and Gudmundson, 2008; Kulachenko and Uesaka, 2012) and textiles (Kato et al., 1997; Sharma and Sutcliffe, 2004; Zohdi and Powell, 2006; Ben Boubaker, 2007a,b; Beex et al., 2012b). The discrete elements in lattice models naturally represent the discrete fibers and yarns of these materials. Therefore, lattice models intrinsically capture discrete mechanical phenomena that occur at the mesoscale or microscale, such as fiber fracture, failure of interfiber bonds and fiber sliding. Even global phenomena such as large rotations of yarns are naturally incorporated in lattice models, whereas these are complex to include in continuum descriptions of fibrous materials (Peng and Cao, 2005; Ten Thije et al., 2007).

Also the mechanical microscale behavior of other materials, for which a discrete representation seems not directly relevant, are nowadays often modeled with lattice models and discrete networks. Reasons are the simplicity and intrinsic discreteness of lattice models and the ability to capture highly anisotropic behavior. Failure of concrete is for instance regularly modeled using lattice models (Chen and Baker, 2003; Lilliu and Van Mier, 2006), whereas they are also used to investigate polymer behavior (Ostoja-Starzewski and Wang, 2006; Rinaldi et al., 2008; Jin and Wang, 2009; Zhao, 2012) and delamination of thin films (Vellinga et al., 2008).

A disadvantage is the computational cost for physically relevant macroscale lattice computations (Lilliu and Van Mier, 2006), since lattice models are constructed at the level of the mesoscale or microscale. Consequently, macroscale lattice computations have a large number of degrees of freedom (DOFs) which makes their governing equations inefficient to solve. The second cause of large computational costs is the computational effort to construct the large number of governing equations.

Multiscale techniques can be adopted to increase the efficiency of large-scale structural lattice computations. Stylianopoulos and Barocas (2007)

have used a classical homogenization scheme for a lattice model of a collagen network. Classical homogenization schemes are able to capture macroscale properties such as the effective stiffness from the mesoscale lattice model, but they are unable to capture local discrete events such as the fracture of an individual fiber. Individual failure events are important to include in mechanical models because they are the precursors of macroscale failure of fibrous materials. In another multiscale approach, continuum descriptions in coarse domains are coupled to lattice models in regions of interest. This is for instance used by Ha-Minh et al. (2011) to model ballistic impact of a woven textile. Failure of discrete fibers and bonds can be modeled by such a multiscale scheme in regions where the lattice model is used. Disadvantages are that the required continuum models for fibrous materials are not trivial to formulate (as mentioned before) and the non-trivial procedures to couple continuum regions to discretely resolved lattice regions.

Other multiscale approaches that are promising for structural lattice models (using trusses and beams) are frameworks that increase the efficiency of atomistic lattice computations. Like structural lattice models, atomistic lattice models include discrete interactions. Several of these (Curtin and Miller, 2003; Xiao and Belytschko, 2004; Fish et al., 2007) also combine continuum descriptions with lattice models, also involving a considerable complexity. The quasicontinuum (QC) method (Tadmor et al., 1996a) however, only relies on the lattice model and is successfully used for atomistic lattice computations (Tadmor et al., 1996b; Miller et al., 1998; Miller and Tadmor, 2002; Kulkarni et al., 2008; Kwon et al., 2009). Conveniently, a continuum description is thus not required. Several QC methods still require a coupling procedure for the internal interface between coarse domains and fully resolved domains of interest - due to the use of the Cauchy-Born rule which is local (Tadmor et al., 1996a,b; Shenoy et al., 1999; Shimokawa et al., 2004). However, some avoid this internal interface (Knap and Ortiz, 2001; Eidel and Stukowski, 2009; Gunzburger and Zhang, 2010; Beex et al., 2012a,c). A number of QC methodologies are therefore potentially convenient for structural lattice models and discrete networks. In the study of Beex et al. (2011) a QC approach without internal interface has been developed to deal with (conservative) structural lattice models.

In the recent work of Beex et al. (2012c), a QC framework has been proposed that is based on the virtual-power statement of non-conservative structural lattice models since many structural lattice models include dissipation. This is in contrast to other QC methods (Eidel and Stukowski, 2009;

Beex et al., 2011, 2012a) developed for conservative atomistic lattice models that are based on energy minimization and cannot deal with dissipative lattice models. Using a virtual-power approach, non-conservative lattice forces can be directly inserted in the QC framework of Beex et al. (2012c). This has been shown for a structural lattice model with elastoplastic trusses.

The aim of this work is to extend the approach to be able to deal with interfiber bond failure and subsequent frictional fiber sliding.

The failure of interfiber bonds (and subsequent fiber sliding) is an important cause of failure of fibrous materials. Different studies have been carried out to investigate bond failure in paper networks (Heyden, 2000; Isaksson and Hägglund, 2007; Hägglund and Isaksson, 2008; Liu et al., 2010; Kulachenko and Uesaka, 2012). Bond failure for a nonwoven glass structure was modeled by Ridruejo et al. (2010) and fiber sliding (i.e. slippage) in textiles was investigated by Zhu et al. (2007). Here, a refined version of the lattice model for bond failure and subsequent fiber sliding of Wilbrink et al. (2012) is used. Instead of the small-sliding formulation of Wilbrink et al. (2012), we use an expression for the energy stored in the lattice that allows for large sliding displacements. Furthermore, our model is rate-dependent instead of the rate-independent case considered by (Wilbrink et al., 2012).

The same type of linear interpolation is used for the sliding displacements (internal history variables) as for the regular displacements (kinematic variables). Consequently, the summation rule of Beex et al. (2012b), in which only one internal sampling point in each interpolation triangle is selected, can still be used. The extension of the virtual-power-based QC framework is validated by comparing the results of multiscale QC examples, in which bond failure and subsequent fiber sliding occur, to the results of direct lattice computations.

The outline of the paper is as follows. First the lattice model of Wilbrink et al. (2012) is reformulated, including a viscous dissipation and an energy expression that allows for large sliding displacements. In the subsequent section, the main principles of the virtual-power-based QC method are considered, as well as the incorporation of the lattice model for bond failure and fiber sliding. In Section 4, multiscale examples are shown and their results are compared to those of the direct lattice computations. Finally, conclusions and recommendations are presented in Section 5.

2. Lattice thermodynamics for bond failure and fiber sliding

QC frameworks increase the efficiency of lattice computations by means of interpolation of the displacements and summation rules to approximate the governing equations instead of resolving them exactly - this is discussed in more detail in the next section. Using summation rules, the potential energy (in this framework the virtual-power) of only a small number of lattice points (so-called sampling points) is determined, instead of determining the potential energy (or virtual-power) of all lattice points. Structural lattice models must be thermodynamically consistent so that no errors occur in the potential energy (or virtual-power) of these sampling points. The reason is that the error in a sampling point is also present in the lattice points that are represented by the sampling point. This can result in a poor accuracy. The formulation of a thermodynamically consistent structural lattice model including bond failure and fiber sliding is therefore first considered along the lines of Germain (1973), as well as a possible solution strategy.

The lattice model considered in this study is an equidistant X-braced network with linear elastic trusses, see Fig. 1. It can be observed that in general every lattice point (i.e. a truss node) is connected to eight neighboring points. Lattice points are only present at crossings of horizontal, vertical and diagonal trusses and not at the locations where only diagonal trusses cross each other. The trusses that are located on the same line can be regarded as fibers or yarns of a fictitious fibrous material. An individual fiber or yarn is thus modeled by a chain of trusses (as the dashed lines in Fig. 1). As a result, fibers are oriented in four directions in the considered lattice. Some of the fibers in the lattice are of a finite length, which can be observed in Fig. 1 by the disconnected curves. A missing truss can be interpreted as the end or start of a fiber, or as an initially broken fiber.

In each lattice point four fibers are connected to each other. A lattice point can therefore be regarded as the collection of four interfiber bonds. Each of these bonds are modeled such that they can fail, leading to frictional sliding of the fibers (trusses) through the nodes (see Fig. 2). A certain sliding force has to be achieved to accommodate fiber sliding after bond failure has taken place. After the deformation is removed, the sliding displacements through the nodes remain present. Consequently, the energy associated with bond failure and frictional sliding, is lost. This entails that bond failure and sliding are dissipative mechanisms.

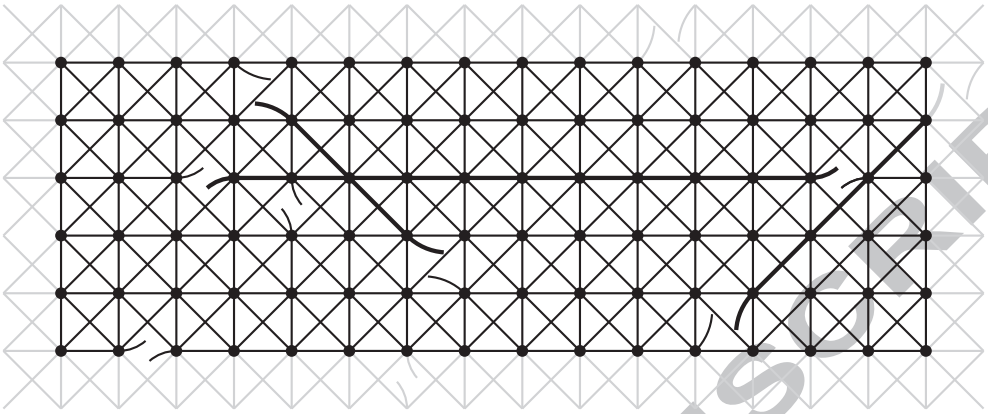

Figure 1: Part of an equidistant X-braced lattice model with linear elastic trusses that can slide through nodes if bonds fail. A number of truss interactions are initially not present. At these locations, half of a truss remains connected to each node. This is indicated by the disconnected curves. To show that each fiber is modelled by a chain of springs, three fibers are presented by thick solid lines.

Figure 2: A part of a fiber (or yarn in textile for instance) shown as a black solid line is modeled by a chain of trusses of which only the truss between nodes i and j is completely shown. The other trusses connected to the nodes are shown in grey. Trusses that belong to the same fiber are presented by the same line style (e.g. dashed and dotted). The different sliding displacements of the black fiber through nodes i and j are indicated by arrows.

2.1. A thermodynamical formulation for non-conservative truss networks

The two-dimensional lattice model in Fig. 1 only contains trusses. The kinematic variables are the displacement components of the lattice points. These are stored in column matrix $\mathbf{u}$ of size $2n \times 1$. Here, n refers to the number of lattice points of the entire lattice, which are stored in index set $N = \{1, ..., n\}$.

For a thermodynamically consistent lattice model, the internal power

equals the external power for an arbitrary variation of the kinematic variables, which is expressed as follows:

$$\dot{\mathbf{u}}^{T\,int}\mathbf{F} = \dot{\mathbf{u}}^{T\,ext}\mathbf{F} \qquad \forall\dot{\mathbf{u}}, \tag{1}$$

where $\dot{\mathbf{u}}^{T\,int}\mathbf{F}$ is the internal power, ${}^{int}P$, and $\dot{\mathbf{u}}^{T\,ext}\mathbf{F}$ the externally applied power. The column matrices containing the decomposed internal forces and external forces are represented by ${}^{int}\mathbf{F}$ and ${}^{ext}\mathbf{F}$, respectively. They are both of size $2n \times 1$. The internal power is the rate of energy stored in the lattice, $\dot{E}$, and the rate of energy dissipated by the lattice, $\dot{D}$, according to the first law of thermodynamics:

$${}^{int}P = \dot{E} + \dot{D}. \tag{2}$$

For a dissipative lattice model the stored energy is a function of the kinematical variables, $\mathbf{u}$, and a set of internal history variables, $\mathbf{z}$, i.e. $E = E(\mathbf{u}, \mathbf{z})$. These internal variables are associated with z dissipation mechanisms in the lattice that are stored in index set $Z = \{1, ..., z\}$. Consequently, $\mathbf{z}$ is of size $z \times 1$. The rate of the stored energy can be formulated using the chain rule according to:

$$\dot{E} = \dot{\mathbf{u}}^T \frac{\partial E}{\partial \mathbf{u}} + \dot{\mathbf{z}}^T \frac{\partial E}{\partial \mathbf{z}}. \tag{3}$$

Substitution of Eq. (3) in Eq. (2) leads to the following expression for the rate of dissipation:

$$\dot{D} = \dot{\mathbf{u}}^T \left({}^{int}\mathbf{F} - \frac{\partial E}{\partial \mathbf{u}} \right) - \dot{\mathbf{z}}^T \frac{\partial E}{\partial \mathbf{z}}. \tag{4}$$

Since the second law of thermodynamics requires the dissipation to be constant or increase, the rate of dissipation can only be zero or positive, i.e. $\dot{D} \geq 0$. It is assumed that only a change of the internal history variables leads to a change of dissipation, i.e. $\dot{D} = 0$ if $\dot{\mathbf{z}} = \mathbf{0}$. To ensure that this is the case for any rate of the kinematic variables, the following relation is formulated for the internal forces:

$$^{int}\mathbf{F} = \frac{\partial E}{\partial \mathbf{u}}. \tag{5}$$

The term between brackets in Eq. (4) vanishes and the formulation of the rate of dissipation in Eq. (4) reduces to:

$$\dot{D} = \dot{\mathbf{z}}^T \, ^z\mathbf{F} \geq 0, \tag{6}$$

with

$$^z\mathbf{F} = -\frac{\partial E}{\partial \mathbf{z}}. \tag{7}$$

Now any dissipation potential Φ is allowed as long as $\dot{D} \geq 0$. The formulation of the dissipation potential is, together with the formulation of the energy stored in the lattice, E, the only ingredient yet to determine. They both depend on the mechanical behavior to describe and are formulated below for the lattice model including bond failure and subsequent frictional fiber sliding. These two formulations differ from those proposed by Wilbrink et al. (2012), where only small sliding displacements are allowed. Moreover, a continuous dissipation potential will be considered here.

2.2. Incorporation of bond failure and subsequent sliding

First, the stored energy, E, is expressed as a function of $\mathbf{u}$ and $\mathbf{z}$ for the case including bond failure and fiber sliding. If half of the energies stored in each truss are projected on node i, the energy of node i, E^i, can be expressed as:

$$E^i = \sum_{j \in B^i} \frac{1}{2} E^{ij}, \tag{8}$$

where E^{ij} represents the energy stored in the truss connecting lattice point i and j. The subset B^i ($B^i \subseteq N$) contains the neighboring points of point i and can thus contain a maximum of eight nodes for the presented lattice

model. By considering all n points of the lattice, the energy stored in the entire lattice, E, can be established according to:

$$E = \sum_{i=1}^{n} E^i = \sum_{i=1}^{n} \sum_{j \in B^i} \frac{1}{2} E^{ij}. \tag{9}$$

The mechanical behavior of each truss in the lattice is linear elastic. The Young's modulus Y and the cross-sectional area of each truss A are chosen independent of the deformation, i.e. they remain constant. The same Young's modulus and area are used for all trusses. Consequently, the energy stored in a linear elastic truss between points i and j, E^{ij}, can expressed as follows:

$$E^{ij} = \frac{1}{2} Y A \, {}^{rel}L^{ij} (\epsilon^{ij})^2 = \frac{1}{2} Y A \, {}^{rel}L^{ij} \left(\frac{{}^{def}L^{ij}}{{}^{rel}L^{ij}} - 1 \right)^2, \tag{10}$$

where ${}^{rel}L^{ij}$ is the relaxed length of the truss between nodes i and j, i.e. the length of the interaction between points i and j that remains after the deformation is removed. The axial elastic strain acting on the relaxed length of the truss is represented by ϵ^{ij}, which is expressed in terms of ${}^{rel}L^{ij}$ and ${}^{def}L^{ij}$, where ${}^{def}L^{ij}$ is the deformed length of the truss between nodes i and j.

Expressions for the relaxed length, ${}^{rel}L^{ij}$, and the deformed length, ${}^{def}L^{ij}$, are trivially extracted from the geometry in Fig. 3. The internal history variables, $\mathbf{z}$, are defined as the sliding displacements that remain after the deformation has been removed (see Fig. 3). Since in each of the n lattice nodes eight trusses, representing four fibers, are bonded, four dissipative sliding mechanisms can occur in each lattice node (see Fig. 1 and Fig. 2). Hence, the number of components z of $\mathbf{z}$ equals $z = 4n$. Based on Fig. 3, the length of the interaction between nodes i and j that remains after deformation is removed, ${}^{rel}L^{ij}$, can be formulated according to:

$${}^{rel}L^{ij} = ||\vec{x}^j - \vec{x}^i|| + z_p - z_q, \tag{11}$$

where $\vec{x}^i$ and $\vec{x}^j$ are the original location vectors of lattice point i and j, rexpectively. z_p is that particular component of $\mathbf{z}$ which characterises the

sliding displacement of the truss between nodes i and j with respect to node i; likewise, z_q characterises the sliding of the same fiber segment with respect to node j. Each sliding displacement is a scalar ($z_p \in \mathbb{R} \quad \forall p \in Z$), since sliding always takes place in the axial direction of the trusses in the lattice model (see Fig. 3) and one therefore should not regard the z_p as a (cartesian) component of a vector $\mathbf{z}$ in space. The length of the interaction between nodes i and j during deformation, ${}^{def}L^{ij}$, trivially reads:

$$ {}^{def}L^{ij} = ||\vec{x}^j + \vec{u}^j - \vec{x}^i - \vec{u}^i||, \tag{12} $$

where $\vec{u}^i$ refers to the displacement vector of lattice point i (see Fig. 3).

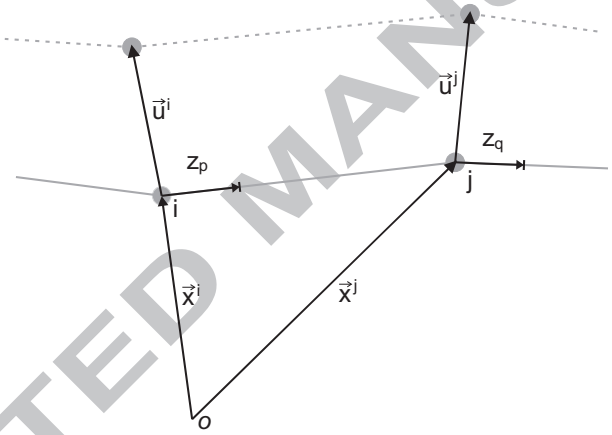

Figure 3: A truss between nodes i and j in the deformed configuration (dashed, grey) and in the relaxed configuration after sliding has occurred through both nodes (solid, grey).

By substitution of Eq. (11) & (12) in Eq. (10), the following expression is obtained that relates E^{ij} - and also E via Eq. (9) - to $\mathbf{u}$ and $\mathbf{z}$:

$$ E^{ij} = \frac{1}{2} Y A (||\vec{x}^j - \vec{x}^i|| + z_p - z_q) \left(\frac{||\vec{x}^j + \vec{u}^j - \vec{x}^i - \vec{u}^i||}{||\vec{x}^j - \vec{x}^i|| + z_p - z_q} - 1 \right)^2 . \tag{13} $$

At this point, the only missing ingredient of the thermodynamical formulation of the lattice model is the dissipation potential, Φ. In principal, the same dissipation potential of Wilbrink et al. (2012) is used, which is a

straightforward Coulomb friction law. The disadvantage of this is the need of an active set strategy that determines which bonds fail, which depends on user-dependent implementation choices. In this study, a viscous friction law is therefore used. The following dissipation potential is proposed:

$$\Phi = \sum_{p=1}^{z} \Phi^p = \sum_{i=1}^{n} \sum_{p \in C^i} \Phi^p \tag{14}$$

with

$$\Phi^p = {}^{z}F_p - {}^{c}F_p \frac{2}{\pi} \tanh(\kappa \dot{z}_p) = 0, \tag{15}$$

where subset C^i contains the bonds in lattice point i ($C^i \subseteq Z$). Furthermore, ${}^{c}F_p$ is the pth component of ${}^{c}\mathbf{F}$, which is the column matrix of size $z \times 1$ containing the critical force values at which bond failure occurs as well as subsequent sliding. Parameter κ is a measure for the slope of the arc tangent function that approaches the Coulomb friction law. The value of $2/\pi$ normalizes the arc tangent. The viscous formulation in Eq. (15) implicitly assumes that all bonds are always active and the solution algorithm is free of user choices. Note furthermore that since $\text{sign}(z_p) = \text{sign}({}^{c}F_p \frac{2}{\pi} \tanh(\kappa \dot{z}_p))$, the condition for the dissipation in Eq. (6) is met for each bond and thus also for the sum of all bonds.

The nonlocality of the presented dissipation formulation can be recognized in the term ${}^{z}F_p$ (equal to $-\partial E / \partial z_p$) in Eq. (15) for bond p. This term depends not only on the sliding displacement of this bond, z_p, but also on the sliding displacements of two bonds adjacent to bond p which are connected to the same fiber.

2.3. Solution procedure

The system of equations resulting from the thermodynamical formulation that need to be solved are the virtual-power statement in Eq. (1) and the dissipation constraints (see Eq. (15)). The governing equations can be expressed according to:

$$\dot{\mathbf{u}}^T {}^{int}\mathbf{F}(\mathbf{u}, \mathbf{z}) = \dot{\mathbf{u}}^T {}^{ext}\mathbf{F} \qquad \forall \dot{\mathbf{u}} \tag{16}$$

$$\dot{\mathbf{z}}^T \left(\mathbf{F}(\mathbf{u}, \mathbf{z}) - \mathbf{M}(\mathbf{z})\, {}^c\mathbf{F} \right) = \mathbf{0}, \tag{17}$$

where $\mathbf{M}$ is a diagonal matrix of size $z \times z$ ($4n \times 4n$) that contains the dissipation equation of each bond on one of its diagonal entries (see also Eq. (20) & (23) further on).

Eq. (16) & (17) can be solved simultaneously using a Newton-Raphson procedure, requiring a consistent linearization. This results in the following expressions:

$$\dot{\mathbf{u}}^T \left({}^{int}\mathbf{F}({}^*\mathbf{u}, {}^*\mathbf{z}) + {}^{int}\mathbf{K}({}^*\mathbf{u}, {}^*\mathbf{z})\, d\mathbf{u} \right) = \dot{\mathbf{u}}^T\, {}^{ext}\mathbf{F} \qquad \forall \dot{\mathbf{u}} \tag{18}$$

$$\dot{\mathbf{z}}^T \left({}^z\mathbf{F}({}^*\mathbf{u}, {}^*\mathbf{z}) - \mathbf{M}({}^*\mathbf{z})\, {}^c\mathbf{F} + \left({}^z\mathbf{K}({}^*\mathbf{u}, {}^*\mathbf{z}) - \frac{\partial \mathbf{M}({}^*\mathbf{z})\, {}^c\mathbf{F}}{\partial \mathbf{z}} \right) d\mathbf{z} \right) = \mathbf{0}, \tag{19}$$

where ${}^*\mathbf{u}$ and ${}^*\mathbf{z}$ are the displacement components and sliding displacements of the previous iteration, respectively. The corrections on the displacement components and sliding displacements are represented by $d\mathbf{u}$ and $d\mathbf{z}$, respectively. The matrices ${}^{int}\mathbf{F}$, ${}^{int}\mathbf{K}$, ${}^z\mathbf{F}$, ${}^z\mathbf{K}$, $\mathbf{M}$ and $\frac{\partial \mathbf{M}\, {}^c\mathbf{F}}{\partial \mathbf{z}}$ are assembled from the contributions of each node:

$${}^{int}\mathbf{F} = \sum_{i=1}^{n} {}^{int}\mathbf{F}^i \qquad {}^{int}\mathbf{K} = \sum_{i=1}^{n} {}^{int}\mathbf{K}^i$$

$${}^z\mathbf{F} = \sum_{i=1}^{n} {}^z\mathbf{F}^i \qquad {}^z\mathbf{K} = \sum_{i=1}^{n} {}^z\mathbf{K}^i$$

$$\mathbf{M}\, {}^c\mathbf{F} = \sum_{i=1}^{n} \sum_{p \in C^i} \mathbf{M}^p\, {}^c\mathbf{F} \qquad \frac{\partial \mathbf{M}\, {}^c\mathbf{F}}{\partial \mathbf{z}} = \sum_{i=1}^{n} \sum_{p \in C^i} \frac{\partial \mathbf{M}^p\, {}^c\mathbf{F}}{\partial \mathbf{z}}, \tag{20}$$

with

$${}^{int}F_k^i = \frac{\partial E^i}{\partial u_k} \qquad {}^{int}K_{kl}^i = \frac{\partial^2 E^i}{\partial u_l \partial u_k}, \tag{21}$$

where k and l run over all $2n$ components of $\mathbf{u}$ and with

$$ {}^{z}F^{i}_{p} = \frac{-\partial E^{i}}{\partial z_p} \qquad {}^{z}K^{i}_{pq} = \frac{-\partial^2 E^{i}}{\partial z_q \partial z_p}, \tag{22} $$

where p and q run over all $4n$ components of $\mathbf{z}$ and with

$$ M^{p}_{pp} = \frac{2}{\pi}\tanh(\kappa \dot{z}_p) \qquad \left(\frac{\partial \mathbf{M}^{p}\,{}^{c}\mathbf{F}}{\partial \mathbf{z}}\right)_{pp} = \frac{\partial (\mathbf{M}^{p}\,{}^{c}\mathbf{F})_{p}}{\partial z_p}. \tag{23} $$

For clarity the external forces are left out of consideration.

Dirichlet boundary conditions are used for $\mathbf{u}$ and $\mathbf{z}$ (required for the nonlocal plastic formulation). Neumann boundary conditions are incorporated in ${}^{ext}\mathbf{F}$. Even though possible, no Neumann boundary conditions are adopted for the nonlocal plastic formulation. To resolve the viscous terms in $\mathbf{M}$ and $\partial \mathbf{M}\,{}^{c}\mathbf{F}/\partial \mathbf{z}$ in Eq. (19), a backward Euler scheme is used, since implicit schemes are more stable than explicit schemes.

The procedure to simultaneously solve the governing equations in Eq. (18) & (19) is computationally inefficient for lattice models with a large number of n lattice nodes. The reason for this is twofold. First, the total system contains $6n$ DOFs, of which $2n$ DOFs are associated with the displacement components and $4n$ DOFs with the sliding displacements. This is a substantial number since n is significant for large-scale lattice computations. Large systems are inefficient to solve, even if Cholesky decomposition or an iterative solver is used. Moreover, the effort associated with the construction of the governing equations in Eq. (18) & (19) is significant, since all n lattice points have to be visited according to the formulations in Eq. (20).

3. Virtual-power-based QC method with a mixed formulation

The QC method has originally been developed for large-scale atomistic lattice computations (Tadmor et al., 1996a), aiming to remedy the two aforementioned causes of high computational cost. The QC method uses two reduction steps for this (see Fig. 4). First, the number of displacements is reduced by means of interpolation (see the center image in Fig. 4). Second, the potential energy, or here the virtual-power, (i.e. the governing equations) is approximated by sampling the potential energy, or the virtual-power, of a small number of sampling points, instead of determining it exactly by visiting all lattice points (see the second step in Fig. 4). In both reduction

steps an error may be introduced that influences the potential energy, or virtual-power, and thus the obtained solution. If both steps are performed adequately however, these errors are negligibly small.

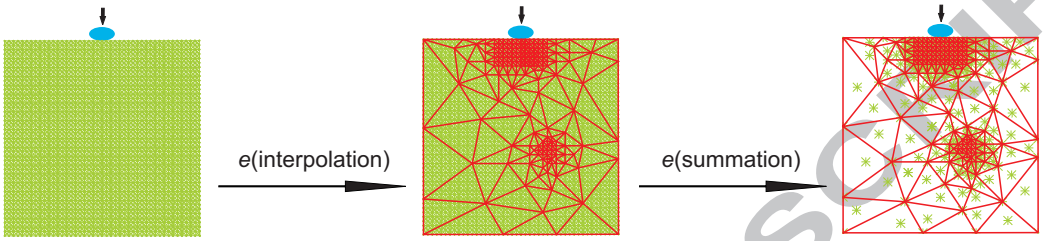

Figure 4: Schematic representation of the two reduction steps in the QC method. In the left image, the full lattice model is shown. In the center image, a triangulation is superimposed to the lattice model and in the right image a small number of lattice points is depicted, which are used to sample the potential energy, or virtual-power (i.e. the governing equations). During both reduction steps an error, e, may be introduced.

3.1. Interpolation

Interpolation in QC methodologies applies to lattice models by the use of interpolation triangles (see the center image in Fig. 4). The interpolation triangles are spanned by the same interpolation functions as used in finite element (FE) methods. Consequently, well established techniques developed for FE methods, e.g. adaptive meshing, can be used in QC methodologies. In general, linear interpolation triangles are used in QC frameworks. The triangle nodes of the interpolation triangles coincide with a limited number of lattice points. These lattice points represent the displacement of the entire lattice and are often referred to as reppoints or repnodes (or repatoms if used for atomistic lattice models). The remaining lattice points are interpolated between the reppoints. Consequently, their displacements entirely depend on the displacements of the reppoints.

The advantage of using interpolation triangles is that in regions in which small displacement fluctuations are expected, the reppoints can be chosen far away from each other. This results in relatively large triangles in which a large number of lattice nodes are constrained and a large reduction of displacements takes place. In regions in which large displacement fluctuations are expected, all the lattice points are selected as reppoints (triangle nodes), i.e. the exact lattice model is captured in these regions. In Fig. 4, two fully

resolved regions are present. One is located in the region where an indenter makes contact with the lattice and the other is located near a lattice defect (e.g. a failed truss).

The r reppoints, stored in index set R, are selected from set N containing all n lattice points, i.e. $R \subseteq N$. To achieve a substantial computational gain, the number of reppoints must be significantly smaller than the total number of lattice points ($r \ll n$). The displacements of all lattice points, $\mathbf{u}$, are approximated by the condensed displacements, $\tilde{\mathbf{u}}$, which can be expressed as a function of the displacements of the reppoints, ${}^{r}\mathbf{u}$, as follows:

$$\mathbf{u} \approx \tilde{\mathbf{u}} = {}^{u}\boldsymbol{\Psi}\, {}^{r}\mathbf{u}, \tag{24}$$

where ${}^{u}\boldsymbol{\Psi}$ is the displacement condensation matrix with size $2n \times 2r$ for two-dimensional lattices. It contains the interpolation functions evaluated at the locations of all lattice points.

So far, most QC frameworks are used for (conservative) atomistic lattice models (Tadmor et al., 1996a; Miller et al., 1998; Knap and Ortiz, 2001; Eidel and Stukowski, 2009; Beex et al., 2012a) including only kinematic variables ($\mathbf{u}$). Here, non-conservative lattice models are considered that include internal history variables ($\mathbf{z}$) associated with dissipation. In case the dissipation mechanisms are local, it suffices to use internal history variables that are constant in (the internal parts of) each interpolation triangle. Consequently, they are not (C_0-)continuous across interpolation triangles, whereas this is the case for the condensed displacements. This is shown in previous work on the virtual-power-based QC method (Beex et al., 2012c) for elastoplastic trusses.

In case of a lattice model with bond failure and subsequent frictional sliding, the dissipation mechanisms are nonlocal, because the sliding displacements directly depend on each other. This can be observed in Eq. (17). Since nonlocal dissipation mechanisms exist here, the internal history variables depend on each other and are not constant within an interpolation triangle. To allow the internal history variables ($\mathbf{z}$) to vary within an interpolation triangle, they are interpolated as well. As mentioned before, the interpolation of the internal history variables entails that large interpolation triangles are only permitted to be used in domains with small fluctuations of the kinematic variables as well with small fluctuations of the internal history variables.

The condensed sliding displacements, $\tilde{\mathbf{z}}$, can be expressed in terms of the sliding displacements of the reppoints according to:

$$\mathbf{z} \approx \tilde{\mathbf{z}} = {}^{z}\boldsymbol{\Psi}\,{}^{r}\mathbf{z}, \tag{25}$$

where ${}^{z}\boldsymbol{\Psi}$ is the sliding displacement condensation matrix with size $z \times 4r$ ($4n \times 4r$) and ${}^{r}\mathbf{z}$ is the column matrix of size $4r \times 1$ containing the sliding displacements of the reppoints. The same interpolation functions evaluated at the locations of all lattice points are present in ${}^{z}\boldsymbol{\Psi}$. As a result, the interpolated internal history variables are also (C_0-)continuous of the interpolation triangles. Although the size of ${}^{z}\boldsymbol{\Psi}$ differs from the size of ${}^{u}\boldsymbol{\Psi}$, they both contain the same interpolation function evaluations. Consequently, almost no additional effort is involved in the construction of both ${}^{z}\boldsymbol{\Psi}$ and ${}^{u}\boldsymbol{\Psi}$, compared to the construction of ${}^{u}\boldsymbol{\Psi}$ only.

An important advantage of using the same interpolation for the internal history variables is the fact that no complex interplay between two types of interpolations occurs. Such an interplay may have a substantial influence on the summation rules. Because the same interpolation is used, previously proposed summation rules can still be used, as explained below.

If Eq. (24) & (25) are inserted in Eq. (18) & (19), the following formulations for the condensed governing equations are obtained:

$${}^{r}\dot{\mathbf{u}}^{T}\left({}^{u}\boldsymbol{\Psi}^{T\,int}\mathbf{F} + {}^{u}\boldsymbol{\Psi}^{T\,int}\mathbf{K}\,{}^{u}\boldsymbol{\Psi}\,d\,{}^{r}\mathbf{u}\right) = {}^{r}\dot{\mathbf{u}}^{T}\,{}^{u}\boldsymbol{\Psi}^{T\,ext}\mathbf{F} \qquad \forall\,{}^{r}\dot{\mathbf{u}} \tag{26}$$

$${}^{r}\dot{\mathbf{z}}^{T}\left({}^{z}\boldsymbol{\Psi}^{T}\,{}^{z}\mathbf{F} - {}^{z}\boldsymbol{\Psi}^{T}\,\mathbf{M}\,{}^{c}\mathbf{F} + \left({}^{z}\boldsymbol{\Psi}^{T}\,{}^{z}\mathbf{K}\,{}^{z}\boldsymbol{\Psi} - {}^{z}\boldsymbol{\Psi}^{T}\,\frac{\partial \mathbf{M}\,{}^{c}\mathbf{F}}{\partial \mathbf{z}}\,{}^{z}\boldsymbol{\Psi}\right)d\,{}^{r}\mathbf{z}\right) = \mathbf{0}. \tag{27}$$

Note that the term ${}^{z}\boldsymbol{\Psi}^{T}$ in the terms ${}^{z}\boldsymbol{\Psi}^{T}\,{}^{z}\mathbf{F}$ and ${}^{z}\boldsymbol{\Psi}^{T}\,{}^{z}\mathbf{K}\,{}^{z}\boldsymbol{\Psi}$ in Eq. (27) originates from substitution of Eq. (25) in Eq. (6). Furthermore, by substitution of Eq. (17) and Eq. (25) in Eq. (6), ${}^{z}\boldsymbol{\Psi}^{T}$ is also introduced in Eq. (27) in the terms ${}^{z}\boldsymbol{\Psi}^{T}\mathbf{M}\,{}^{c}\mathbf{F}$ and ${}^{z}\boldsymbol{\Psi}^{T}\frac{\partial \mathbf{M}\,{}^{c}\mathbf{F}}{\partial \mathbf{z}}\,{}^{z}\boldsymbol{\Psi}$.

The terms ${}^{u}\boldsymbol{\Psi}^{T\,int}\mathbf{F}$, ${}^{u}\boldsymbol{\Psi}^{T\,int}\mathbf{K}\,{}^{u}\boldsymbol{\Psi}$, ${}^{z}\boldsymbol{\Psi}^{T}\,{}^{z}\mathbf{F}$, ${}^{z}\boldsymbol{\Psi}^{T}\,{}^{z}\mathbf{K}\,{}^{z}\boldsymbol{\Psi}$, ${}^{z}\boldsymbol{\Psi}^{T}\mathbf{M}\,{}^{c}\mathbf{F}$ and ${}^{z}\boldsymbol{\Psi}^{T}\frac{\partial \mathbf{M}\,{}^{c}\mathbf{F}}{\partial \mathbf{z}}\,{}^{z}\boldsymbol{\Psi}$ represent the condensed counterparts of the corresponding expressions in Eq. (20). Like their uncondensed counterparts, they can be assembled by contributions of each node:

$$
{}^{int}\tilde{\mathbf{F}} = \sum_{i=1}^{n} {}^{u}\mathbf{\Psi}^{T}\, {}^{int}\mathbf{F}^{i} \qquad {}^{int}\tilde{\mathbf{K}} = \sum_{i=1}^{n} {}^{u}\mathbf{\Psi}^{T}\, {}^{int}\mathbf{K}^{i}\, {}^{u}\mathbf{\Psi}
$$

$$
{}^{z}\tilde{\mathbf{F}} = \sum_{i=1}^{n} {}^{z}\mathbf{\Psi}^{T}\, {}^{z}\mathbf{F}^{i} \qquad {}^{z}\tilde{\mathbf{K}} = \sum_{i=1}^{n} {}^{z}\mathbf{\Psi}^{T}\, {}^{z}\mathbf{K}^{i}\, {}^{z}\mathbf{\Psi}
$$

$$
\tilde{\mathbf{M}}\, {}^{c}\mathbf{F} = \sum_{i=1}^{n} {}^{z}\mathbf{\Psi}^{T} \sum_{p\in C^{i}} \mathbf{M}^{p}\, {}^{c}\mathbf{F}
$$

$$
\frac{\partial \tilde{\mathbf{M}}\, {}^{c}\mathbf{F}}{\partial\, {}^{r}\mathbf{z}} = \sum_{i=1}^{n} {}^{z}\mathbf{\Psi}^{T} \sum_{p\in C^{i}} \frac{\partial \mathbf{M}^{p}\, {}^{c}\mathbf{F}}{\partial \mathbf{z}}\, {}^{z}\mathbf{\Psi}, \tag{28}
$$

where the tilde refers to the condensed counterparts of the force columns and stiffness matrices in Eq. (20).

To ensure that the virtual-power of the condensed system adequately approximates that of the original system, only little difference in the virtual-power of the lattice points may exist. This entails that large interpolation triangles (i.e. coarse domains) can only be used in regions with small displacement fluctuations *and* (in contrast to regular QC methodologies) with small sliding displacement fluctuations. Indeed, linear interpolation enforces that the virtual-power of a lattice point in a large triangle is identical to the value in its neighboring point (i.e. ${}^{r}\dot{\mathbf{u}}^{T}\, {}^{u}\mathbf{\Psi}^{T} \frac{\partial E^{i}}{\partial \mathbf{u}} = {}^{r}\dot{\mathbf{u}}^{T}\, {}^{u}\mathbf{\Psi}^{T} \frac{\partial E^{i+1}}{\partial \mathbf{u}}$). This is only allowed if the virtual-power of these lattice points is nearly equal in the direct lattice model (i.e. $\dot{\mathbf{u}}^{T} \frac{\partial E^{i}}{\partial \mathbf{u}} \approx \dot{\mathbf{u}}^{T} \frac{\partial E^{i+1}}{\partial \mathbf{u}}$).

By means of interpolation the number of governing equations is reduced from $6n$ to $6r$. This makes the condensed system significantly more efficient to solve (assuming that $r \ll n$). However, still all n lattice points need to be visited to construct the condensed governing equations in Eq. (26) & (27) compromizing the computational cost.

3.2. Summation

The second step proposed in the QC method aims to reduce of the computational effort to construct the governing equations. Rather than visiting all n lattice points to construct the governing equations according to Eq. (28), only a small number of s sampling points are selected to sample the virtual-power and thus the the governing equations (see the right step in Fig. 4). This is called summation in QC terminology. The sampling points, stored in subset S, are selected from all lattice points (ie. $S \subseteq N$).

As a result of summation, the expressions for the virtual-power and equality constraints remain the same as in Eq. (26) & (27). The construction of the force columns and stiffness matrices changes however. They are now expressed according to:

$$
\begin{aligned}
{}^{int}\tilde{\tilde{\mathbf{F}}} &= \sum_{i \in S} w^{i\,u} \boldsymbol{\Psi}^T\, {}^{int}\mathbf{F}^i \qquad & {}^{int}\tilde{\tilde{\mathbf{K}}} &= \sum_{i \in S} w^{i\,u} \boldsymbol{\Psi}^T\, {}^{int}\mathbf{K}^{i\,u} \boldsymbol{\Psi} \\
{}^{z}\tilde{\tilde{\mathbf{F}}} &= \sum_{i \in S} w^{i\,z} \boldsymbol{\Psi}^T\, {}^{z}\mathbf{F}^i \qquad & {}^{z}\tilde{\tilde{\mathbf{K}}} &= \sum_{i \in S} w^{i\,z} \boldsymbol{\Psi}^T\, {}^{z}\mathbf{K}^{i\,z} \boldsymbol{\Psi} \\
\tilde{\tilde{\mathbf{M}}}\, {}^{c}\mathbf{F} &= \sum_{i \in S} w^{i\,z} \boldsymbol{\Psi}^T \sum_{p \in C^i} \mathbf{M}^{p\,c}\mathbf{F} \\
\frac{\partial \tilde{\tilde{\mathbf{M}}}\, {}^{c}\mathbf{F}}{\partial^r \mathbf{z}} &= \sum_{i \in S} w^{i\,z} \boldsymbol{\Psi}^T \sum_{p \in C^i} \frac{\partial \mathbf{M}^{p\,c}\mathbf{F}}{\partial \mathbf{z}}\, {}^{z}\boldsymbol{\Psi}, \qquad (29)
\end{aligned}
$$

where w^i is the weight factor of sampling point i, which equals the number of lattice points that are represented by sampling point i (including sampling point i itself). The combination of the bar and the tilde refers to the summed, condensed counterparts of the force columns and stiffness matrices. Furthermore, the weight factor w^i is introduced in the formulations of $\tilde{\tilde{\mathbf{M}}}\, {}^{c}\mathbf{F}$ and $\frac{\partial \tilde{\tilde{\mathbf{M}}}\, {}^{c}\mathbf{F}}{\partial^r \mathbf{z}}$ to ensure that in the summed, condensed system the same amount of dissipation occurs as in the condensed system (see Eq. (26) & (27)).

Summation in the QC method is only computationally beneficial if the number of sampling points is substantially smaller than the number of lattice points in the full lattice model ($s \ll n$). Furthermore, to ensure a sufficient

accuracy of the QC method (i.e. to ensure that the summed, condensed governing equations are a good representation of the condensed governing equations), sampling points must be selected such that the virtual-power of the sampling points approximates that of the lattice points they represent. This entails that if for two neighboring lattice points in a large triangle ${}^{r}\dot{\mathbf{u}}^{T}\,{}^{u}\boldsymbol{\Psi}^{T}\frac{\partial E^{i}}{\partial \mathbf{u}} \approx {}^{r}\dot{\mathbf{u}}^{T}\,{}^{u}\boldsymbol{\Psi}^{T}\frac{\partial E^{i+1}}{\partial \mathbf{u}}$, then one of them can be used to sample the virtual-power of the other lattice point.

The way in which the sampling points are selected, the computation of their weight factors and the manner in which their potential energy, or here virtual-power, are determined (locally or nonlocally) are established in so-called summation rules. Two general classes of summation rules can be distinguished. Local-nonlocal summation rules (Tadmor et al., 1996a,b; Miller et al., 1998; Shenoy et al., 1999; Shimokawa et al., 2004) compute the potential energy (here virtual-power) of sampling points in coarse domains in a local fashion. In the fully resolved region the sampling points are treated in a nonlocal fashion, so that the exact lattice model is captured in these regions. Local-nonlocal summation rules come with internal interfaces between coarse and fully resolved domains. Corrective procedures have been formulated for the interfaces (Shenoy et al., 1999; Shimokawa et al., 2004), involving additional assumptions.

Nonlocal summation rules treat all sampling points in a nonlocal fashion (Knap and Ortiz, 2001; Eidel and Stukowski, 2009; Gunzburger and Zhang, 2010; Beex et al., 2011, 2012a). As a consequence, no internal interface occurs between coarse domains and fully resolved domains. Therefore, no interface corrections are required. The relatively large lookup tables that are involved can be considered as a disadvantage, but the fact that no corrective procedures are required (and updated during remeshing) is a computational advantage. More information on summation rules can be found for instance in the papers of Miller and Tadmor (2002); Eidel and Stukowski (2009) and Beex et al. (2012a).

The summation rule employed in this study is the central summation rule (Beex et al., 2012a), because it uses a small number of sampling points ($s \ll n$) resulting in a high efficiency. Furthermore, since all sampling points are treated in a nonlocal fashion, no internal interface occurs. In the central summation rule, only one lattice point near the incenter of each triangle is selected as an internal sampling point representing all lattice points inside the triangle and half of those on triangle edges (this number determines its corresponding weight factor, $w^{i} \geq 1$), see Fig. 5. The reppoints are selected

as discrete sampling points, i.e. they only sample themselves ($w^i = 1$). As a result, the exact lattice model is recovered in the fully resolved regions as desired. Lattice points in triangles in which no internal lattice points occurs, i.e. all lattice points of a triangle are located on triangle edges, are selected as discrete sampling points as well (see Fig. 5). Hence, for the central summation rule, it holds that $R \subseteq S \subseteq N$.

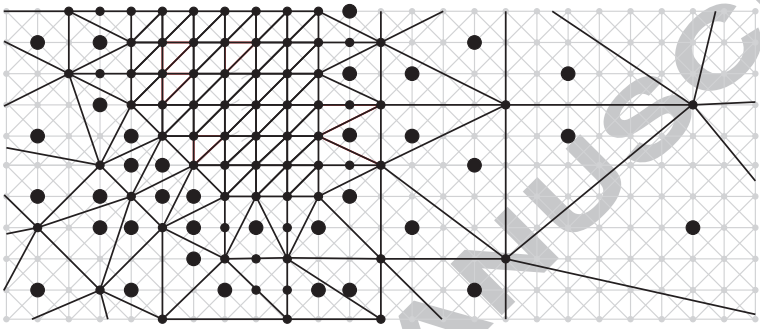

Figure 5: The central summation rule applied to the lattice model (grey) with a triangulation (black) that includes a fully resolved region around three missing horizontal interactions. The discrete sampling points (with $w^i = 1$) are shown as black dots and internal sampling points (with $w^i \geq 1$) as large black dots.

The central summation rule is appropriate to sample the virtual-power in the QC framework presented here, because its fundamental principle also holds for the mixed formulation proposed here. The ansatz of the central summation rule is that, except near triangle edges (Beex et al., 2011, 2012a), the potential energies of all lattice points within an interpolation triangle are equal, because each type of interaction (e.g. the horizontal interactions) deforms the same inside a triangle due to the linear interpolation used. Since in the method proposed here, the same linear interpolation is used for the displacements as well as the sliding displacements, each type of interaction fully inside a triangle deforms in the same way, which is the main principle of the central summation rule.

4. Performance of the QC framework

Two numerical test cases are considered to illustrate the computational gain and accuracy that can be achieved with the proposed QC framework for bond failure and frictional fiber sliding. Both numerical cases have a true multiscale character since local mesoscale lattice defects (a small number of

initially missing trusses) are present in an otherwise perfectly regular large-scale network. The numerical examples are formulated in a dimensionless setting. All parameters are normalized by the lattice spacing in horizontal and vertical direction, which are equal to each other.

4.1. Problem description

In both numerical examples the proposed QC method is used for a lattice model containing 99×99 unit cells (see Fig. 6). The considered lattice model is based on the equidistant X-braced lattice model with linear elastic trusses as formulated in Section 2, whereby only horizontal trusses (fibers) can slide through lattice points. The horizontal and vertical lengths of a unit cell are set to 1 (lattice spacing). Diagonal trusses are thus of length $\sqrt{2}$ (lattice spacing). In the lower center of the model, 25 horizontal trusses are missing, starting from the bottom of the model (see Fig. 6). These 25 horizontal fibers can thus be regarded as initially broken. The fiber (truss) overlengths at these points are so large that no pull-out occurs in the computations.

All bond strengths (and thus also all critical friction forces) are set to 1. This means that all components of ${}^{c}\mathbf{F}$ in Eq. (15) & (19) equal 1. Furthermore, the parameter defining the arc tangent function in Eq. (15), κ, is set to 100. The stiffness per unit of length of all trusses (YA in Eq. (13)) is set to 10^6 in the first example and to 10^3 in the second example. In this way, sliding displacements in a large number of points are expected in the first example and only a few points are expected to slide in the second example.

The boundary conditions applied to the model are shown in Fig. 6 as well. In the QC computations the boundary conditions are applied to reppoints and in the direct lattice computations they are applied to lattice points. It may be clear that the points on the left edge are fixed in horizontal (x-)direction and vertical (y-)direction (see Fig. 6). The points on the top, bottom and right edge are fixed in y-direction. The points on the right edge are displaced in horizontal direction. Furthermore, the sliding displacements of the points on the left and right edges of the model are constrained. The results shown below are obtained using 1000 increments.

4.2. Computational efficiency

The computational efficiency of a QC framework directly depends on the triangulation used. A fully resolved region is used in the domain in which significant sliding displacement fluctuations are expected. This is the case close to the removed trusses, where large sliding displacement fluctuations

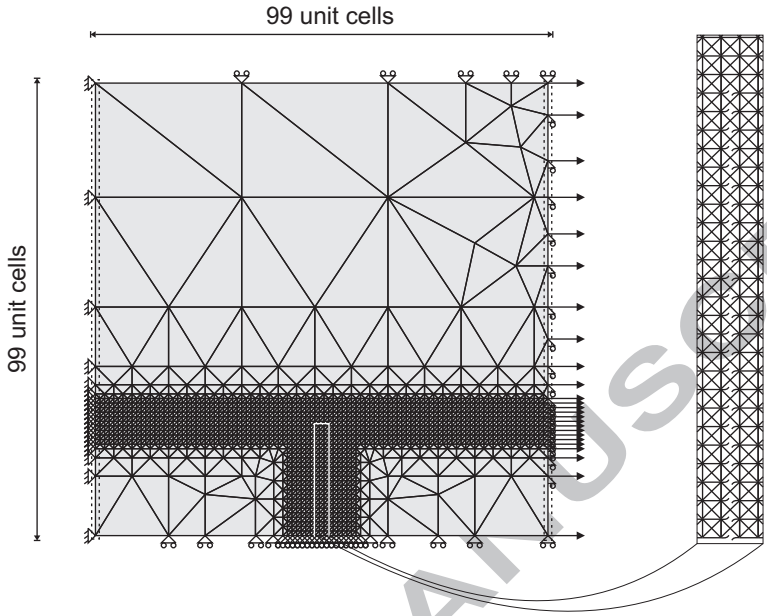

Figure 6: Schematic representation of the numerical examples including the adopted triangulation. The boundary conditions on the sliding displacements are shown by dashed rectangles at the left and right edges. The zoom on the right shows the central vertical row with missing trusses without interpolation triangles. Diagonal fiber segments (trusses) are still present.

are triggered, since the stiffness of the trusses is large compared to the bond strength. Furthermore, it is expected that negligible sliding displacements occur in the region above the centrally removed trusses. Therefore, a discrete step in the sliding displacements (large sliding displacement fluctuations) is expected over the entire width of the model at a height of 24 lattice spacings. Since this cannot be accurately resolved by large interpolation triangles, this region is also fully resolved.

In the direct lattice computation 10,000 lattice points are involved, resulting in 30,000 DOFs, of which 20,000 DOFs for the displacement components and 10,000 for the horizontal sliding displacements. In the triangulation in Fig. 6, a relatively large number of reppoints is present because of the relatively large fully resolved domain. Accordingly, also a large number of sampling points is involved, since every reppoint is a discrete sampling point as well (with $w^i = 1$). In total 1,655 reppoints are present in the triangulation of Fig. 6 and 2,140 sampling points (see also ahead to the right image

in Fig. 7). Hence, the computational gain obtained by the QC framework is a factor of 6 in terms of DOFs (associated with the effort to solve the governing equations) and a factor of 5 in terms of sampling points (related to the computational cost to construct the governing equations). The expected computational gain is clearly significant, even though a relatively large part of the model is fully resolved.

4.3. Accuracy

The sliding displacements predicted by the direct lattice computation and the QC computation are presented in Fig. 7 for an applied macroscopic horizontal strain of 1.5% (corresponding to an applied horizontal displacement of 1.485 in terms of lattice spacings). The stiffness per unit of length of each truss equals 10^6. Significant sliding displacements occur in the domains next to the vertical row of missing trusses. No sliding displacements are present above this domain.

Fig. 7 reveals that the sliding displacements predicted by the QC computation with the triangulation shown in Fig. 6 are similar to those predicted by the direct lattice computation. This includes the sliding near the missing trusses and the discrete jump across a horizontal line above them. This accurate solution essentially results from the use of a fully resolved region where needed. The sliding displacements predicted by the QC computation in the coarse domain on the left and right of the vertical row with missing trusses are adequately captured (see Fig. 7). Note that if the sliding displacements would not be interpolated and kept constant in each triangle (as done for the dissipation variables by Beex et al. (2012c)), the sliding displacement field would not be resolved accurately.

The fact that the sliding displacements are accurately captured in the entire domain, is emphasized by the left plot in Fig. 8, in which the discrepancies between the sliding displacements predicted by the QC computation and direct lattice computation (i.e. $\tilde{\tilde{\mathbf{z}}} - \mathbf{z}$) are shown on the entire model domain. The maximum difference is approximately 0.003, which is small compared to the predicted sliding displacements (which have a maximum absolute value of approximately 0.73 as can be seen in Fig. 7). Quantifying this difference, based on the sliding displacements of all 25 nodes on the left side of the vertical row with horizontal trusses removed, shows that the average relative error is only 0.004%. Although the difference is small compared to the predicted sliding displacements, the difference between the sliding displacement is largest in the two corners around the fully resolved

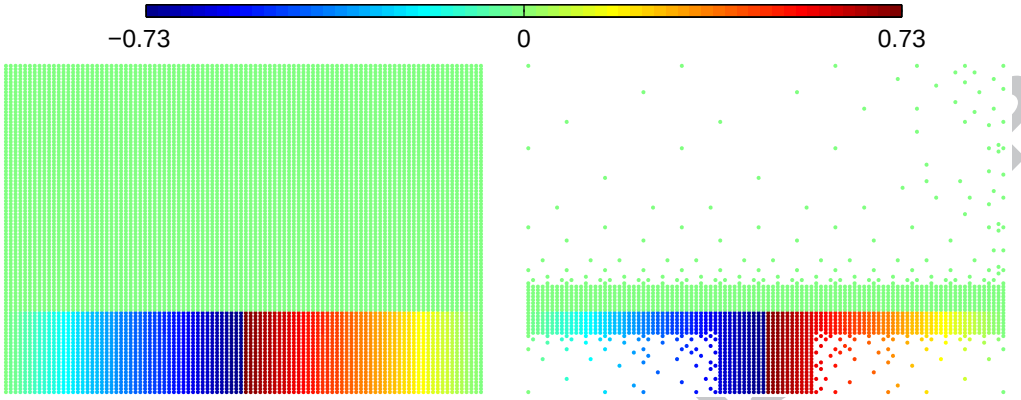

Figure 7: Horizontal sliding displacements in the lattice - stiffness per unit of length of each truss is 10^6. Left: direct lattice computation, right: QC computation.

domain. Also in the top region of the fully resolved domain a difference can be observed. This spurious effect is most likely caused by the use of the fully nonlocal central summation rule employed Beex et al. (2012a).

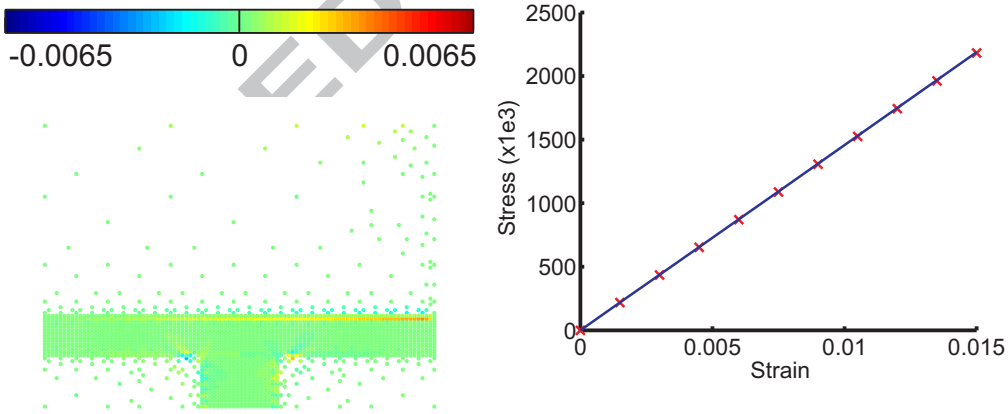

Figure 8: Left: discrepancy between the sliding displacements predicted by the direct lattice computation and QC computation (stiffness per unit of length of each truss 10^6). The colors represent the discrepancy of the sliding displacements ($\tilde{\mathbf{z}} - \mathbf{z}$). Note that the same colorbar is used as in Fig. 11. Right: stress-strain curves predicted by the direct lattice computation (line) and the QC computation (x).

To illustrate that the global response is also accurately captured by the QC framework, macroscopic stress-strain curves of the QC computation and direct lattice computation are presented in the right diagram of Fig. 8. The relative error of the stress at the maximum strain is 0.33%.

In Fig. 9 the relative horizontal displacements of the lattice points are presented (in terms of lattice spacings). The horizontal displacements relative to the defect free configuration, ${}^{rel}u$, are determined according to:

$$ {}^{rel}u(\vec{x}^i) = {}^{x}u(\vec{x}^i) - {}^{xx}Ex^i, \tag{30} $$

where ${}^{xx}E$ is the applied overall strain in x-direction and x^i is the horizontal component of the position vector of point i.

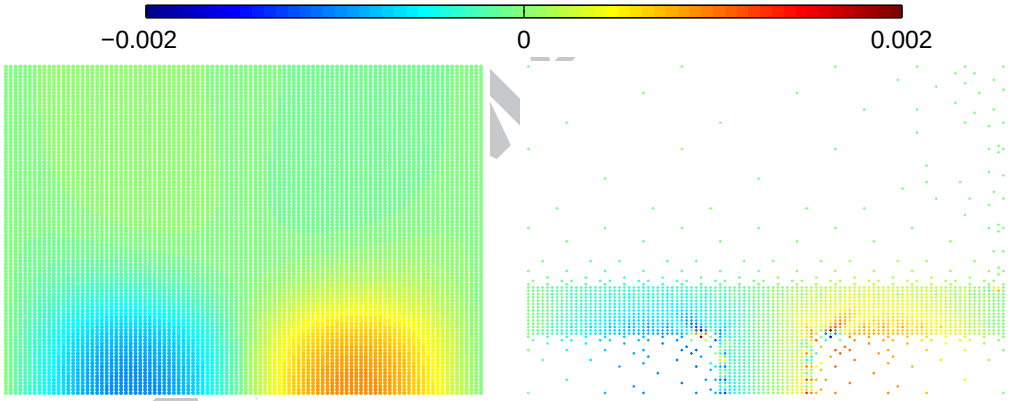

Figure 9: The relative horizontal displacements in the lattice (stiffness per unit of length of each truss 10^6) predicted by the direct lattice computation (left) and the QC computation (right).

Fig. 9 reveals that the minimum and maximum relative horizontal displacements are located between the center and the edges of the model and not in the center as one might expect. This results from the fact that sliding occurs in all lattice points associated with the first 25 horizontal fibers, starting from the bottom of the model. The QC computation is able to capture this relative displacement field relatively well, but not exactly, as can be seen on the right in Fig. 9. These displacements are resolved in relatively large triangles and they do not vary exactly linearly within these triangles.

The accuracy of the displacements is thus not as good as that of the sliding displacements with this triangulation. Adaptivity - i.e. remeshing of these domains - can be used to improve the accuracy of the relative displacement field, if these local fluctuations are to be resolved more accurately.

The predicted sliding displacements for the second case, in which the stiffness per unit of length is 10^3, are shown in Fig. 10 for the same applied macroscopic horizontal strain of 1.5%. Overall, the sliding displacements predicted by the direct lattice computation and QC simulation are similar. Sliding displacements occur only in the lattice points in and near the vertical row of missing trusses due to the substantially smaller stiffness of the trusses. With a stiffness that is 1000 times smaller than in the first example, significantly larger truss deformations - requiring substantially larger macroscopic horizontal strains - are required to obtain substantial sliding in a significant amount of lattice points.

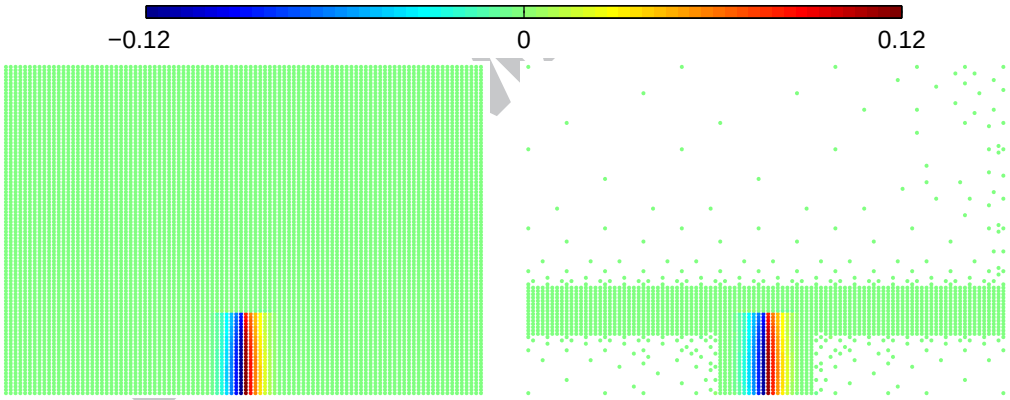

Figure 10: Horizontal sliding displacements in the lattice (stiffness per unit of length of each truss 10^3) predicted by the direct lattice computation (left) and the QC computation (right).

The difference between the sliding displacements resulting from the QC computation and the direct lattice computation is presented in the left image of Fig. 11. The discrepancy is more substantial compared to the first test case, but nevertheless quite small. After all, the maximum absolute discrepancy is only 0.0065, whilst the maximum absolute sliding displacement is 0.12. For example, the average relative error based on the 25 nodes directly on the left of the vertical row with horizontal missing trusses is only 2.3%.

It is remarkable that the discrepancy is larger for the second example, in which non-zero sliding displacements only seem to be present in the fully resolved domain, whereas in the first example, non-zero sliding displacements are clearly present in the fully resolved region and coarse domain. This is due to the small sliding displacements that are present in coarse domains in the second example. The left diagram in Fig. 11 reveals no sliding displacements in the solution of the direct lattice computation. However, because the dry friction is modeled continuously in this framework, small sliding displacements are also present here, influencing those in the fully resolved domain. Separate computations (not shown here) indicate that these sliding displacements are not linearly distributed in space. Consequently, the mixed formulation framework in which the sliding displacements are linearly interpolated is not able to fully capture these non-linear small sliding displacements. This explains why the accuracy in the fully resolved region in the second example is less good compared to the first example, even though sliding displacements are only noticeable in the fully resolved domain in the second example.

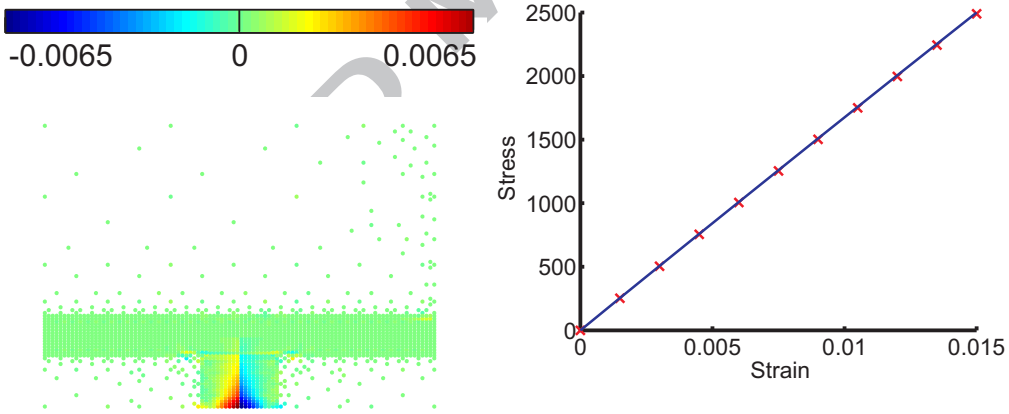

Figure 11: Left: discrepancy between the sliding displacements predicted by the direct lattice computation and QC computation (stiffness per unit of length of each truss 10^3). The colors represent the discrepancy of the sliding displacements ($\tilde{\mathbf{z}} - \mathbf{z}$). Note that the same colorbar is used as in Fig. 8. Right: The macroscopic stress predicted by the direct lattice computation (line) and the QC computation (x) as a function of the horizontal strain.

The stress-strain curves shown in the right diagram of Fig. 11 are also for

this test virtually identical. At the maximum strain, the absolute relative error of this force is only 0.42%. Hence, also the global response is captured well in this case.

The relative horizontal displacements, computed using Eq. (30), for the second example at an applied macroscopic horizontal strain of 1.5% are shown in Fig. 12. In contrast to the first example, they clearly show their minimum and maximum values close the vertical row with missing trusses. This is caused by the fact that (significant) sliding is only present in this domain. Since the most pronounced relative horizontal displacements are present in the fully resolved domain, they are generally better captured by the QC model than in the first example. However, non-zero relative horizontal displacements also occur in coarse domains, which are not that accurately captured. Here as well, adaptive remeshing can be used if such local details are of interest.

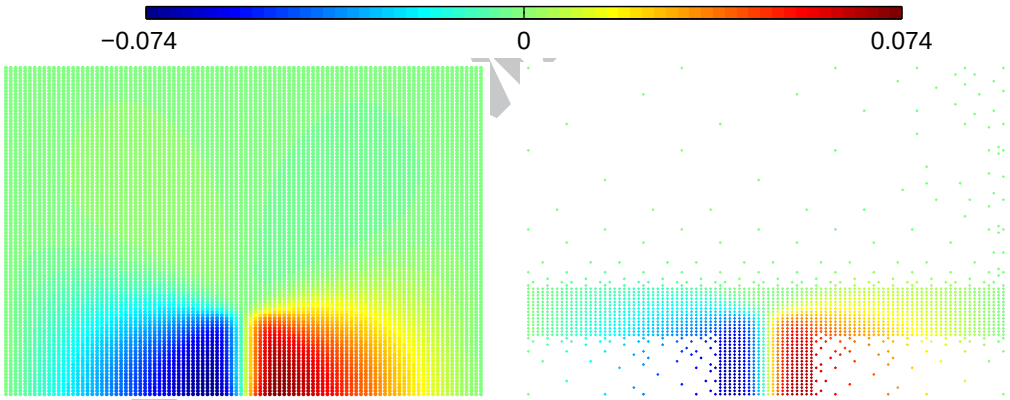

Figure 12: The relative horizontal displacements in the lattice (stiffness per unit of length of each truss 10^3) predicted by the direct lattice computation (left) and the QC computation (right).

5. Conclusion

Lattice models employing trusses and beams can straightforwardly and accurately describe mechanical mesoscale phenomena of fibrous materials. Bond failure, including subsequent frictional fiber sliding, is one of these

mesoscale phenomena that are important for the (macroscale) failure behavior of several fibrous materials. The disadvantage of lattice models is the computational cost for macroscale (the engineering scale) computations, because of their solution and construction at the mesoscale. Different multiscale techniques can be used to decrease the computational effort of lattice models, but they all have their specific scope. In this study, the quasicontinuum (QC) method is adopted for lattice models with bond failure and subsequent fiber sliding. The QC method

- allows the incorporation of the full discrete lattice model in regions of interest,
- completely relies on the underlying discrete lattice model and not on a homogenized continuum description that is difficult to obtain for dissipative fibrous materials, and
- does not require a coupling or handshaking procedure (in the proposed framework).

QC methods are based on (i) interpolation of the lattice displacements to decrease the number of degrees of freedom and (ii) summation rules in which a small number of lattice points is sampled to approximate the governing equations. Most QC methods are based on energy minimization and cannot deal with dissipative mechanisms, which are intrinsic to lattice models with bond failure and fiber sliding. To this end, a previously proposed virtual-power-based QC method (Beex et al., 2012c) is exploited that can deal with dissipative (non-conservative) lattice models. In the present paper, the virtual-power-based QC framework is equipped with a mixed formulation, because bond failure and fiber sliding are intrinsically nonlocal dissipative mechanisms and the previously introduced virtual-power-based QC framework can only deal with local dissipative mechanisms.

The internal dissipation variables (the sliding displacements) are interpolated in the proposed methodology, next to the kinematic variables (the regular displacements), ensuring their direct mutual coupling. The same interpolation triangles are used for this, which has the advantage that previously proposed summation rules remain applicable. Consequently, the new QC framework with the mixed formulation has a similar efficiency and accuracy as previously defined QC methodologies.

The consistent derivation of the presented framework ensures that the QC methodology is useful for different fibrous materials. The bond description is straightforward to adjust - by only changing the dissipation potential - so that the approach can directly be used for fibrous materials such as paper and textiles. For this purpose, microstructural experimental identification strategies for inter-fiber bond descriptions are essential research ingredients (Ridruejo et al., 2010; Kulachenko and Uesaka, 2012).

Acknowledgements

This research is supported by the Dutch Technology Foundation STW, which is the applied science division of NWO, and the Technology Programme of the Ministry of Economic Affairs under Project Nr. 10104.

References

Argento, G., Simonet, M., Oomens, C.W.J., Baaijens, F.P.T., 2012, Multi-scale mechanical characterization of scaffolds for heart valve tissue engineering, Journal of Biomechanics, Vol. 45, 2893-2898.

Arnoux, P.J., Bonnoit, J., Chabrand, P., Jean, M., Pithioux, M., 2002, Numerical damage models using a structural approach: application in bones and ligaments, The European Physical Journal of Applied Physics, Vol. 17, 65-73.

Batchelor, W., 2008, An analytical solution for the load distribution along a fibre in a nonwoven network, Mechanics of Materials, Vol. 40, 975-981.

Beex, L.A.A., Peerlings, R.H.J., Geers, M.G.D., 2011, A quasicontinuuum methodology for multiscale analyses of discrete microstructural models, International Journal for Numerical Methods in Engineering, Vol. 86, 701-718.

Beex, L.A.A., Peerlings, R.H.J., Geers, M.G.D., 2012a, Central summation in the quasicontinuum method, Submitted.

Beex, L.A.A., Verberne, C.W., Peerlings, R.H.J., 2012b, Experimental characterization of a lattice model for woven materials: application to electronic textile, Composites Part A: Applied Science and Manufacturing, Vol. 46, 82-92.

Beex, L.A.A., Peerlings, R.H.J., Geers, M.G.D., 2012c, A multiscale quasicontinuum method for dissipative lattice models and discrete networks, Submitted.

Bronkhorst, C.A., 2003, Modelling paper as a two-dimensional elastic-plastic stochastic network, International Journal of Solids and Structures, Vol. 40, 5441-5454.

Ben Boubaker, B., Haussy, B., Ganghoffer, J.F., 2007a, Discrete woven structure model: yarn-on-yarn friction, C.R. Mecanique, Vol. 335, 150-158.

Ben Boubaker, B., Haussy, B., Ganghoffer, J.F., 2007b, Considerations of the yarn-yarn interactions in meso/macro discrete model of fabric Part II: Woven fabric under uniaxial and biaxial extension, Mechanics Research Communications, Vol. 34, 371-378.

Chandran, P.L., Barocas, V.H., 2007, Affine versuse non-afinne fibril kinematics in collagen networks: theoretical studies of network behavior, Journal of Biomechanical Engineering, Vol. 128, 259-270.

Chen, G., Baker, G., 2003, Influence of bond slip on crack spacing in numerical modeling of reinforced concrete, Journal of Structural Engineering, Vol. 129, 1514-1521.

Cui, X., Zhang, Y., Zhao, H., Lu, T.J., Fang, D., 2011, Stress concentration in two-dimensional lattices with imperfections, Acta Mechanica, Vol. 216, 105-122.

Curtin, W.A, Miller, R.E., 2003, Atomistics/continuum coupling in computational materials science, Modelling and Simulation in Materials Science and Engineering, Vol. 11, 33-68.

Eidel, B., Stukowski, A., 2009, A variational form of the quasicontinuum method based on energy sampling in clusters, Journal of the Mechanics and Physics of Solids, Vol. 57, 87-108.

Fish, J., Nuggehally, M.A., Shephard, M.S., Picu, C.R., Badia, S., Parks, M.L., Gunzburger, M., 2007, Concurrent AtC coupling based on a blend of the continuum stress and the atomistic force, Computer Methods in Applied Mechanics and Engineering, Vol. 196, 4548-4560.

Germain, P., 1973, The method of virtual power in continuum mechanics Part 2: microstructure, SIAM Journal on Applied Mathematics, Vol. 25, 556-575.

Gunzburger, M., Zhang, Y., 2010, A quadrature-rule type approximation to the quasi-continuum method, Multiscale Modeling and Simulation, Vol. 8, 571-590.

Hägglund, R., Isaksson, P., 2008, On the coupling between macroscopic material degradation and interfiber bond fracture in an idealized fiber network, International Journal of Solids and Structures, Vol. 45, 868-878.

Ha-Minh, C., Kanit, T., Boussu, F., Imad, A., 2011, Numerical multi-scale modeling for textile woven fabric against ballistic impact, Computational Materials Science, Vol. 50, 2172-2184.

Hatami-Marbini, H., Picu, R.C., 2009, An eigenstrain formulation for the prediction of elastic moduli of defective fiber networks, European Journal of Mechanics A/Solids, Vol. 38, 305-316.

Heyden, S., 2000, Network modelling for the evaluation of mechanical properties of cellulose fibre fluff, Doctoral thesis, Lund University, Lund, Sweden.

Hou, X., Acar, M., Silberschmidt, V.V., 2009, 2D finite element analysis of thermally bonded nonwoven materials: continuous and discontinuous models, Computational Materials Science, Vol. 46, 700-707.

Intrigila, B., Melatti, I., Tofani, A., Macchiarelli, G., 2007, Computational models of myocardial endomysial collagen arrangement, Computer Methods and Programs in Biomedicine, Vol. 86, 232-244.

Isaksson, P., Hägglund, R., 2007, Evoluation of bond fractures in a randomly distributed fiber network, International Journal of Solids and Structures, Vol. 44, 6135-6147.

Jin, Y.J., Wang, T.J., 2009, Three-dimensional numerical modeling of the damage mechanism of amorphous polymer network, Computational Materials Science, Vol. 46, 632-638.

Kato, S., Minami, H., Yoshino, T., Namita, T., 1997, Analysis of membrane structures based on fabric lattice model considering viscous characteristics,

Proceedings of the IASS Symposium 1997 on Shell and Spatial Structures, 411-420, Singapore.

Knap, J., Ortiz, M., 2001, An analysis of the quasicontinuum method, Journal of the Mechanics and Physics of Solids, Vol. 49, 1899-1923.

Kulachenko, A., Uesaka, T., 2012, Direct simulation of fiber network deformation and failure, Mechanics of Materials, Vol. 51, 1-14.

Kulkarni, Y., Knap, J., Ortiz, M., 2008, A variational approach to coarse graining of equilibrium and non-equilibrium atomistic description at finite temperature, Journal of the Mechanics and Physics of Solids, Vol. 56, 1417-1449.

Kwon, S., Lee, Y., Park, J.Y., Sohn, D., Lim, J.H., Im, S. 2009, An efficient three-dimensional addaptive quasicontinuum method using variable-node elements, Journal of Computational Physics, Vol. 228, 4789-4810.

Lilliu, G., Van Mier, J.G.M., 2006, On the relative use of micro-mechanical lattice analysis of 3-phase particle composites, Engineering Fracture Mechanics, Vol. 74, 1174-1189.

Liu, J.X., Chen, Z.T., Li, K.C., 2010, A 2-D lattice model for simulating the failure of paper, Theoretical and Applied Fracture Mechanics, Vol. 51, 1-10.

Miller, R., Ortiz, M., Phillips, R., Shenoy, V., Tadmor, E.B., 1998, Quasicontinuum models of fracture and plasticity, Engineering Fracture Mechanics, Vol. 61, 427-444.

Miller, R.E., Tadmor, E.B., 2002, The quasicontinuum method: overview, applications and current directions, Journal of Computer-Aided Materials Design, Vol. 9, 203-239.

Ngan, A.H.W., 2009, Canonical ensemble for static elastic structures with random microstructures, Journal of the Mechanics and Physics of Solids, Vol. 57, 803-811.

Ostoja-Starzewski, M., Wang, G., 2006, Particle modeling of random crack patterns in epoxy plates, Probabilistic Engineering Mechanics, Vol. 21, 267-276.

Peng, X.Q., Cao, J., 2005, A continuum mechanics-based non-orthogonal constitutive model for woven composite fabrics, Composites: Part A, Vol. 36, 859-874.

Ridruejo, A., Gonzalez, C., LLorca, J., 2010, Damage micromechanisms and notch-sensitivity of glass fiber nonwoven felts: an experimental and numerical study, Journal of the Mechanics and Physics of Solids, Vol. 58, 1628-1645.

Rinaldi, A., Krajcinovic, D., Peralta, P., Lai, Y.C., 2008, Lattice models of polycristalline microstructures: a quantitative approach, Mechanics of Materials, Vol. 40, 17-36.

Ryvkin, M., Slepyan, L., 2010, Crack in a 2D beam lattice: analytical solution for two bending modes, Journal of the Mechanics and Physics of Solids, Vol. 58, 902-917.

Sharma, S.B., Sutcliffe, M.P.F., 2004, A simplified finite element model for draping of woven material, Composites: Part A, Vol. 35, 637-643.

Shenoy, V.B., Miller, R., Tadmor, E.B., Rodney, D., Phillips, R., Ortiz, M., 1999, An adaptive finite element approach to atomistic scale mechanics-the quasicontinuum method, Journal of the Mechanics and Physics of Solids, Vol. 47, 611-642.

Shimokawa, T., Mortensen, J.J., Schiøtz, J., Jacobsen, K.W., 2004, Matching conditions in the quasicontinuum method: Removal of the error introduced at the interface between the coarse-grained and fully atomistic region, Physical Review B, Vol. 69, 214104.

Silberstein, M.N., Pai, C.L., Rutledge, G.C., Boyce, M.C., 2012, Elastic-plastic behavior of non-woven fibrous mats, Journal of the Mechanics and Physics of Solids, Vol. 60, 295-318.

Strömbro, J., Gudmundson, P., 2008, An anisotropic fibre-network model for mechano-sorptive creep in paper, International Journal of Solids and Structures , Vol. 45, 5765-5787.

Stylianopoulos, T., Barocas, V.H., 2007, Volume-averaging theory for the study of the mechanics of collagen networks, Computer Methods in Applied Mechanics and Engineering, Vol. 196, 2981-2990.

Tadmor, E.B., Ortiz, M., Philips, R., 1996a, Quasicontinuum analysis of defects in solids, Philosophical Magazine A, Vol. 73, 1529-1563.

Tadmor, E.B., Philips, R., Ortiz, M., 1996b, Mixed atomistic and continuum models of deformation in solids, Langmuir, Vol. 12, 4529-4534.

Ten Thije, R.H.W., Akkerman, R., Huétink, J., 2007, Large deformation simulation of anisotropic material using an updated Lagrangian finite element method, Computer Methods in Applied Mechanics and Engineering, Vol. 196, 3141-3150.

Tserper, K.I., Labeas, G.N., 2009, Progressive fracture analysis of planar lattices and shape-morphing Kagome-structure, Theoretical and Applied Fracture Mechanics, Vol. 51, 41-47.

Vellinga, W.P., Van den Bosch, M., Geers, M.G.D., 2008, Interaction between cracking, delamination and buckling in brittle elastic thin films, International Journal of Fracture, Vol. 154, 195-209.

Wilbrink, D.V., Beex, L.A.A., Peerlings, R.H.J., 2012, A discrete network model for bond failure and frictional sliding in fibrous materials, International Journal of Solids and Structures, Vol. 50, 1354-1363.

Xiao, B.K., Belytschko, T., 2004, A bridging domain method for coupling continua with molecular dynamics, Computer Methods in Applied Mechanics and Engineering, Vol. 193, 1654-1669.

Zeman, J., Peerlings, R.H.J., Geers, M.G.D., 2011, Non-local energetics of random heterogeneous lattices, Journal of the Mechanics and Physics of Solids, Vol. 59, 1214-1230.

Zhao, X., 2012, A theory for large deformation and damage interprenetating polymer networks, Journal of the Mechanics and Physics of Solids, Vol. 60, 319-332.

Zhu, B., Yu, T.X., Tao, X.M., 2007, Large deformation and slippage mechanism of plain woven composite in bias extension, Composites: Part A, Vol. 38, 1821-1828.

Zohdi, T.I., Powell, D., 2006, Multiscale construction and large-scale simulation of structural fabric undergoing ballistic impact, Computer Methods in Applied Mechanics and Engineering, Vol. 195, 94-109.